

Cosmic ray mass independent energy reconstruction method using Cherenkov light and muon content in LHAASO

Liping Wang¹, Lingling Ma^{2,3,*}, Shoushan Zhang^{2,3,†}, Cunfeng Feng^{1,‡}, Zhen Cao,^{2,3,4} Liqiao Yin,^{2,3}
Yudong Wang,^{2,3} Jing Zhao,^{2,3} Zhe Li,^{2,3} Lingyu Wang,^{2,3} and Songzhan Chen^{2,3}

¹Key Laboratory of Particle Physics and Particle Irradiation (MOE),
Institute of Frontier and Interdisciplinary Science, Shandong University,
Qingdao, Shandong 266237, China

²Key Laboratory of Particle Astrophysics, Institute of High Energy Physics, Chinese Academy of Sciences,
100049 Beijing, China

³TIANFU Cosmic Ray Research Center, 610213 Chengdu, Sichuan, China

⁴University of Chinese Academy of Sciences, 100049 Beijing, China



(Received 29 December 2022; accepted 8 February 2023; published 28 February 2023)

The wide field-of-view Cherenkov telescope array of the Large High Altitude Air Shower Observatory (LHAASO) measures the longitudinal development of Cherenkov light in the air shower of cosmic rays, while the kilometer-square array of LHAASO measures the number of muons in the air shower. The unique detector arrangement of LHAASO can facilitate the precise reconstruction of the cosmic ray energy in the knee region. Thus, this study proposed a new energy reconstruction method by simultaneously using the Cherenkov light size and the number of muons, which is insensitive to the primary particle type. Using this method, the energy bias and resolution of the light component (proton and helium) were less than 1% and 10% at approximately 1 PeV, respectively. Moreover, the difference in energy bias between helium and proton was less than 1% at approximately 1 PeV. In addition, the dependence of this energy reconstruction method on hadronic interaction models and cosmic ray components was also discussed.

DOI: [10.1103/PhysRevD.107.043036](https://doi.org/10.1103/PhysRevD.107.043036)

I. INTRODUCTION

Despite the discovery of cosmic rays more than 100 years ago, their origin, acceleration, and propagation mechanisms remain unclear. It is generally believed that galactic cosmic rays originate from supernova remnants because they can provide the energy required for cosmic ray acceleration. The measurement of the cosmic ray energy spectra of individual components near the “knee” region can aid in the understanding of the origin and acceleration mechanism of cosmic rays. The flux of cosmic rays decreases rapidly with increasing energy, and the measurement of high-energy cosmic rays with energies around the knee region through spaceborne experiments is nearly impossible owing to their limited effective area. Moreover, they are mainly reliant on the measurements of the extensive air shower (EAS) induced by cosmic rays on the ground. To date, many studies have attempted to determine the composition of cosmic rays with energies around the knee, including KASCADE [1], Tibet AS- γ [2], ARGO-YBJ [3], and the prototype of the Large High

Altitude Air Shower Observatory and the wide field-of-view Cherenkov Telescope Array (LHAASO-WFCTA) [4]. However, their results were inconsistent. One reason for this is that the measurement of the primary energy and primary mass of an observed EAS is entangled. Thus, a mass composition independent measurement of the primary energy is key to measuring the energy spectrum of all particles and individual mass groups of cosmic rays.

LHAASO is located on Haizi Mountain in Sichuan, China, 4410 m above sea level, and corresponds to an air depth of 600 g/cm² [5,6]. LHAASO comprises three independent detector arrays: a 78 000 m² water Cherenkov detector array (WCDA), a kilometer-square array (KM2A) with electromagnetic detectors and muon detectors, and WFCTA. With different types of detector arrays, LHAASO can measure multiple parameters of the air showers simultaneously, such as the number of muons and the image of Cherenkov light. This study investigated the method of energy reconstruction by building an energy estimator based on the combined observation of KM2A and WFCTA. This energy reconstruction method exhibited almost mass independence. The combined observation and measurements of muons and Cherenkov light are briefly described in Sec. II. The method to estimate the air shower

*llma@ihep.ac.cn

†zhangss@ihep.ac.cn

‡fengcf@sdu.edu.cn

energy is introduced in Sec. III. Finally, conclusions are presented in Sec. IV.

II. EXPERIMENT AND SIMULATION

A. WFCTA and KM2A detector

The measurement of the energy spectra of individual or mass groups of cosmic rays is a primary goal of LHAASO. To constrain the origin and acceleration models of cosmic rays, the knee positions in the proton and iron energy spectra should be measured accurately, which requires LHAASO to cover the energy range of several hundred TeV to 100 PeV. Thus, the observation of LHAASO-WFCTA is divided into two stages to cover a wide energy range. The first stage is the combined observation of the first six WFCTA telescopes, the first half KM2A array, and the first water pool of WCDA with the aim of measuring the proton and light component (proton and helium) energy spectra in the energy range from several hundred TeV to 10 PeV. The second stage is the combined observation of 18 WFCTA telescopes, the entire KM2A array, and the entire WCDA array with the aim of measuring the iron energy spectrum in the energy range of 10–100 PeV. This study was based on the detector setup of the first stage.

WFCTA has 18 Cherenkov telescopes and is designed to collect and image atmospheric Cherenkov light emitted from charged particles in an air shower [7,8]. The first six telescopes have been in operation since October 2019. They are located in the southwest corner of the first pond of WCDA, as indicated by the black dots in Fig. 1. The elevation of the telescopes was 60° , which corresponds to a slant air depth of 700 g/cm^2 at the observation level.

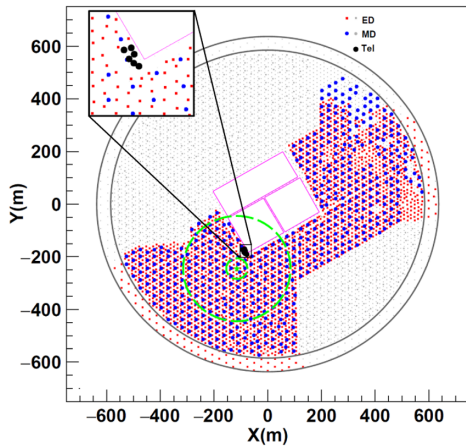


FIG. 1. Layout of the detectors of the first half KM2A and the first six telescopes of WFCTA (see the black dots in the enlarged view). The solid red squares identify the EDs positions, while the solid blue circles indicate the MDs position in the half KM2A array. The central purple squares indicate the WCDA array region. The green star shows the core of one shower, and the green dashed circles show the corresponding muon-counting rings of 40–200 m radius.

Together with 12 other telescopes, these six telescopes were moved to the southeast corner of the first pool of WCDA. A total of 18 telescopes have been in operation since May 2021. The elevation of the 18 telescopes is set to 45° for higher-energy observations.

The half and full arrays of KM2A began operations in January 2020 and July 2021, respectively. The half array of KM2A comprises 2365 electromagnetic detectors (EDs) and 578 muon detectors (MDs), as shown in Fig. 1 (squares and circles, respectively). The EDs and MDs are distributed with spacings of 15 and 30 m, respectively. Detailed descriptions of the KM2A setup can be found in Refs. [5,9]. The combined reconstruction of events with KM2A and WFCTA can be performed through an off-line procedure based on the trigger time recorded by the two detector arrays.

B. Simulation

Extensive air shower events were generated by CORSIKA (7.4000 version) [10]. To simulate the combined observation of KM2A and WFCTA, the Cherenkov option was turned on, and both the Cherenkov information and secondary particle information of each air shower were recorded. The hadronic interaction model QGSJET-II-04 [11] was chosen as the baseline event generator, whereas the EPOS-LHC [12] model was chosen for model validation.

Five mass compositions of hydrogen (proton), helium, nitrogen (CNO group), aluminum (MgAlSi group), and iron were generated. All five mass composition groups were generated in two energy ranges 100 TeV–1 PeV and 1–10 PeV, following a power-law function with a spectral index of -1 to increase the statistics of high-energy events. The fluxes of the five composition groups were weighted using the Gaisser (H3a) [13] composition model. Because the first six WFCTA telescopes were set as 30° in the zenith direction, the zenith angle was sampled in the range of 20° – 40° and the azimuth angle was sampled in the range of 95° – 275° to cover the field of view of the six telescopes. The total number of simulated EAS for QGSJET-II-04 and EPOS-LHC hadronic interaction models was approximately 1.47×10^7 and 5.73×10^6 , respectively.

Detector simulations of KM2A and WFCTA were performed independently based on the same EAS. The attenuation of Cherenkov light caused by Rayleigh scattering, aerosol scattering, and ozone absorption was considered based on the American standard atmospheric model in the simulation of the WFCTA. Further, the response of the telescopes was studied through the tracking of the propagation process of photons in the telescope, including the sheltering of the camera and container of the telescope, reflectivity of the mirrors, and light funnels. To simulate the response of KM2A detectors, G4KM2A [14], based on GEANT4 (V4.10.00) [15] has been developed. In this study, the configuration of KM2A was set as the half array of KM2A in the simulation.

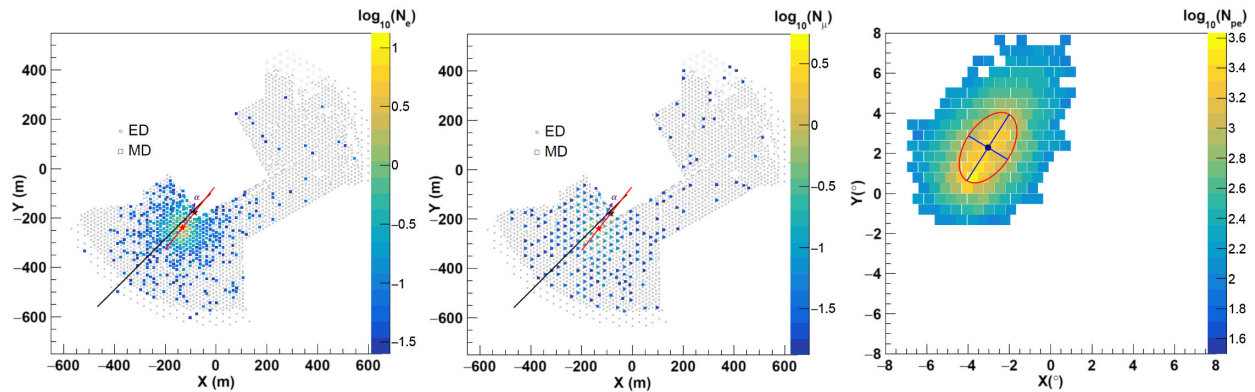


FIG. 2. A combined event recorded by both KM2A and WFCTA. Left: the electromagnetic particle number map recorded by EDs. Middle: the muon number map recorded by MDs. Right: a Cherenkov image recorded by WFCTA. The color accords to the logarithm of the number of detected electromagnetic particles (left), the number of detected muons (middle), and photoelectron (right). The red and black stars connected by the red lines in the left and middle panels indicate the core of the air shower reconstructed by KM2A and the position of the telescope of WFCTA, respectively. The black lines in the left and middle panels indicate the intersection line between the shower-detector-plane reconstructed by WFCTA and the ground. The major and minor axes of the ellipse in the Cherenkov image indicate the length and width (the Hillas parameters).

A combined event recorded by KM2A and WFCTA simultaneously is shown in Fig. 2. The left and middle plots show the electromagnetic particle number and muon number maps, respectively. The electromagnetic particle number map was used to reconstruct the shower core and direction precisely [16]. The muon number map was used to count the number of muons in the shower. The right plot shows the Cherenkov image of the same shower observed by WFCTA, which provides the information on the photoelectron number in the Cherenkov image of the shower. The reconstructed core from the electromagnetic particles is represented by red stars in the left and middle panels in Fig. 2. Therefore, the combined event can provide multiple parameters [6], such as the total number of Cherenkov lights measured by telescopes and the number of muons detected by MDs.

C. Event selection

To ensure a high quality of the reconstructed shower observables, event selection criteria are applied:

- (1) The reconstruction effects of events near the edge of WCDA were avoided by discarding the events with a reconstructed core within 50 m at the edge of WCDA.
- (2) Only events with reconstructed core positions falling within a perpendicular distance from the telescope to the shower axis (R_p) from 60–120 m were used.
- (3) The intersection angle (α) (the angle between the red and black lines in the left and middle plots of Fig. 2) should be less than 10° to further rule out events with erroneous reconstruction.
- (4) Considering the pointing of the telescopes, showers with zenith angle range 22° – 38° and azimuth angle

range $|\phi - \phi_{\text{tel}}| < 13^\circ$ were selected, where ϕ_{tel} is the pointing of the telescopes.

- (5) The center of gravity (MeanX, MeanY) of the image should be $|\text{MeanX}| < 6^\circ$ and $|\text{MeanY}| < 6^\circ$ to ensure that the Cherenkov images were complete.
- (6) The number of fired EDs should be larger than 20, and the hit number of EDs with filtering out noise should be larger than 10 to ensure a high-quality reconstruction of the shower core and arriving directions.
- (7) The number of fired silicon photomultipliers (SiPMs) should be greater than 10 in the cleaned Cherenkov image.

D. The number of muon measurement

In the LHAASO experiment, the muon content of the air shower can be detected by the MD array with high precision, and the number of muons within the ring 40–200 m from the shower axis (named Ring_{40-200}) is proportional to the total number of muons in the air showers [17]. Therefore, the number of muons, counting the muon over the MDs within Ring_{40-200} , was used in the previous analysis. However, if the shower core closes the WCDA or edge of the MD array, such as the green star shown in Fig. 1, the MD cannot cover the corresponding ring completely owing to the lack of MDs in WCDA or outside the half array. In this case, the measured number of muons is less than that of the completely covered ring and induces a deviation in the analysis results.

To avoid this issue, this study developed a new method to measure the number of muons in Ring_{40-200} . In this method, Ring_{40-200} was divided into eight subrings of 20 m width, and the number of muons N_μ in Ring_{40-200} was calculated as

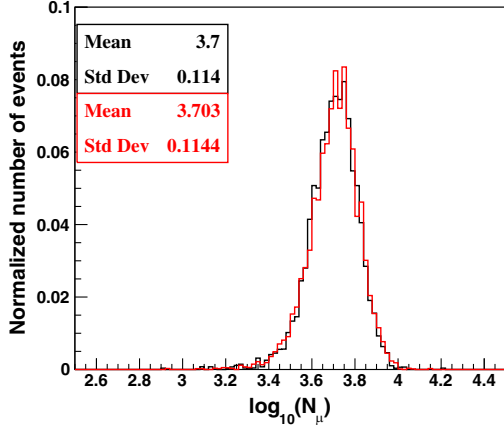


FIG. 3. Distributions of N_μ with the Ring_{40–200} incompletely covered by MD (red line) and the rings completely covered by MD (black line) in the energy range of $E_{\text{true}} 10^{6.0}\text{--}10^{6.2}$ GeV.

$$N_\mu = \sum \frac{N_{\mu,i}}{S_i^{\text{eff}}} \times S_i, \quad (1)$$

where $i = 1 \dots 8$ denotes the i th subring with a width of 20 m in Ring_{40–200}; $N_{\mu,i}$ and S_i^{eff} are the number of measured muons and the sum of the area of all MDs in the i th subring, respectively, and S_i is the geometric area of the i th subring.

Based on this definition, the distribution of the number of muons N_μ is shown in Fig. 3 for showers with the energy of $10^{6.0}\text{--}10^{6.2}$ GeV for two types of event. One type of event with shower core was close to the WCDA or the edge of KM2A, and the MDs do not cover the entire ring Ring_{40–200} completely. Another type of event with shower core was far from any edge of the half KM2A, and the MDs can cover ring Ring_{40–200} almost completely. As shown in Fig. 3, the N_μ distribution is the same for both event types. Thus, this N_μ definition is independent of the ring Ring_{40–200} completely covered by MDs.

E. The Cherenkov light size

The Cherenkov light size (N_{pe}) was measured by counting the photoelectron number of the fired SiPM within the Cherenkov image of the shower event after noise cleaning. Owing to the Cherenkov light lateral distribution, the Cherenkov light size (N_{pe}) is dependent on the perpendicular distance from the telescope to the shower axis (R_p). As shown in Fig. 4, the average N_{pe} decreased with increase in R_p . The normalized Cherenkov light size N_{pe}^0 is defined by R_p correction according to the following formula:

$$\log_{10}(N_{\text{pe}}^0) = \log_{10}(N_{\text{pe}}) + \beta R_p, \quad (2)$$

where the parameter β is obtained by fitting the relationship between N_{pe} and R_p of the light component (proton

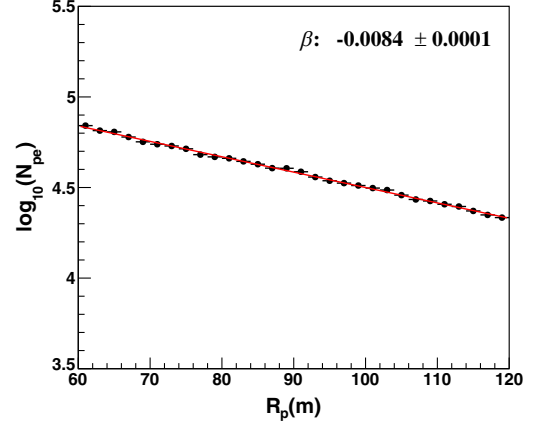


FIG. 4. N_{pe} versus R_p for light component (proton and helium) air showers. The red line is the fitted result of the linear function.

and helium) as shown in Fig. 4. The normalized Cherenkov light size N_{pe}^0 is independent of R_p and was used in the following data analysis.

III. ENERGY RECONSTRUCTION

A. Principle of energy reconstruction

Most Cherenkov light is emitted by the secondary electrons and positrons in the air shower and indicates the electromagnetic energy in the air shower. The air showers initiated by gamma rays are dominated by electromagnetic components; therefore, the Cherenkov light size is a good energy estimator for the energy of gamma rays [18]. The nucleus air shower transfers a part of its energy to the electromagnetic part by π^0 decay. The energy fraction transferred to the electromagnetic part was approximately $[1 - (2/3)^n]$ and the energy fraction remaining in the hadronic part was approximately $(2/3)^n$, where n is the number of interactions in the hadronic air shower [19]. According to the superposition model [20,21], compared to the air shower induced by a light nucleus, that induced by a heavy nucleus has an earlier longitudinal development of showers, and a smaller n is expected. Thus, a heavier nucleus results in a higher-energy fraction remaining in the hadronic part, and a smaller energy fraction is transferred to the electromagnetic part. The Cherenkov light is proportional to the electromagnetic energy; thus, the use of Cherenkov light to reconstruct the energy of the nucleus air shower implies mass composition dependency, as shown in the left panel of Fig. 5. The difference between the energies of the proton and iron reconstructed by the normalized Cherenkov light size was approximately 37% in the energy range of 500–800 TeV, which is similar to Ref. [4].

To reduce the effects of the primary mass in the energy reconstruction using the energy estimator N_{pe}^0 , the energy of the hadronic part should be considered. At the final status of the hadronic air shower, most of the charged pions and

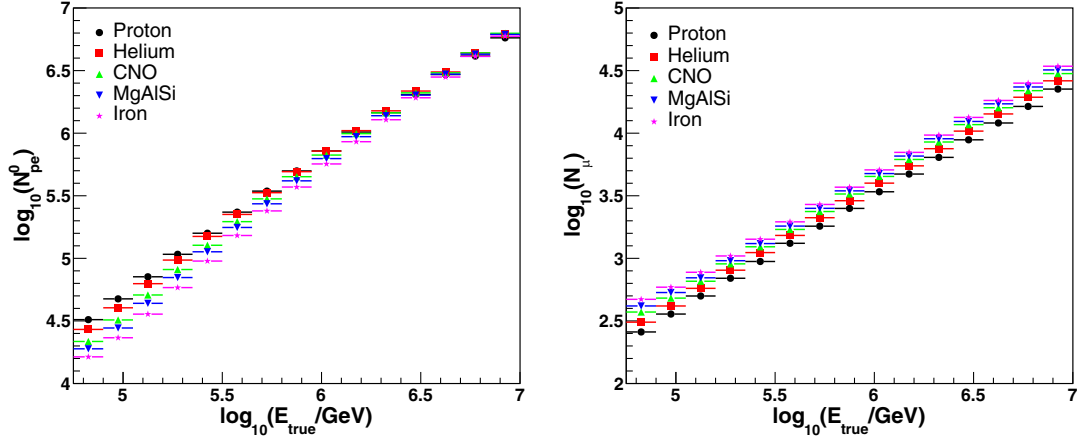


FIG. 5. Normalized Cherenkov light size N_{pe}^0 (left) and the N_{μ} (right) versus E_{true} of the five groups of cosmic rays. Different shapes with different colors are described in the plot.

kaons decay into muons. Thus, the number of muons can represent the energy fraction that remains in the hadronic part. The relationship between the number of muons N_{μ} and the cosmic ray primary energy is shown in the right panel of Fig. 5. The number of muons increased as a function of energy, which is consistent with Ref. [22]. Both N_{μ} and N_{pe}^0 were related to the primary energy of cosmic rays; however, they were affected by the primary particle type.

LHAASO with its combined observation can measure N_{pe}^0 in the Cherenkov image and the number of muons in KM2A, simultaneously. Thus, an energy estimator combining Cherenkov light and muons can be used to reconstruct the primary energy of a nuclear air shower.

B. Energy reconstruction method

In the Heitler-Matthews model [21], the primary energy (E_{true}) of the air shower is derived as

$$E_{true} = g\epsilon_c^e \left(N_e^{max} + \frac{\epsilon_c^{\pi}}{g\epsilon_c^e} N_{\mu}^{max} \right), \quad (3)$$

where N_e^{max} and N_{μ}^{max} are the number of electromagnetic particles and muons in the air shower when the air shower develops to its maximum, $\epsilon_c^e = 85$ MeV and $\epsilon_c^{\pi} = 20$ GeV are the critical energies of electromagnetic particles and pions, respectively, and $g = 10$ is the correction factor in the Heitler-Matthews model.

Equation (3) was derived considering the shower maximum. If the measurement deviates from the shower maximum, the number of electromagnetic particles (N_e) on the observatory will deviate from N_e^{max} because of the fast attenuation of electromagnetic particles in the air shower [23]. Thus, the energy reconstruction accuracy decreases when using N_e . For the ground-based array, determining whether the observed shower is at its

maximum is challenging, particularly for a shower in a wide energy range. The solution is to find a measurable shower observable sensitive to the particle number at the shower maximum position, and this parameter is insensitive to fluctuations in the shower maximum position.

Relativistic charged particles in an air shower traveling through the atmosphere can produce Cherenkov light, and the attenuation of Cherenkov light from the generation point to the observation plane is small [20,24], indicating the insensitivity of Cherenkov light to the position of the air shower maximum. Based on the Monte Carlo (MC) simulation of the light composition, the relationship between the normalized Cherenkov light size N_{pe}^0 and N_e^{max} is shown in the left panel of Fig. 6, which can be well described by $\log_{10}(N_{pe}^0) = \log_{10}(N_e^{max}) + m$, where the parameter $m = 0.079 \pm 0.001$ is obtained by fitting MC data. Therefore, we replace N_e^{max} with N_{pe}^0 .

Muon attenuation in an air shower is also smaller than that in electromagnetic particles [25]. According to the MC simulation, as shown in the right panel of Fig. 6, the relationship between the number of muons N_{μ} measured using Eq. (1) and the number of muons at the shower maximum (N_{μ}^{max}) follows $\log_{10}(N_{\mu}) = \log_{10}(N_{\mu}^{max}) + n$, where the parameter $n = -0.599 \pm 0.001$ was extracted from the fit to the MC simulation.

Based on the above discussion, a composite variable $N_{c\mu}$ was developed for energy reconstruction, which combined the normalized Cherenkov light size (N_{pe}^0) and number of muons (N_{μ}) as follows:

$$N_{c\mu} = N_{pe}^0 + CN_{\mu}, \quad (4)$$

where $C = \epsilon_c^{\pi}/(g\epsilon_c^e) \times 10^m/10^n \approx 120$ is derived with respect to the Heitler-Matthews model [Eq. (3)].

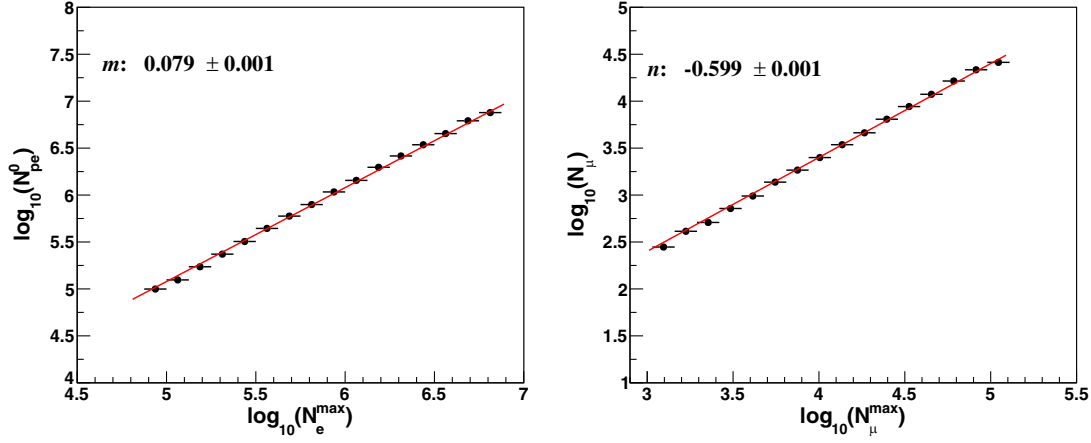


FIG. 6. Left: N_{pe}^0 versus N_e^{\max} of light component. Right: N_μ versus N_μ^{\max} of light component in MC simulation. The red lines are fitted results of the function $\log_{10}(N_{pe}^0) = \log_{10}(N_e^{\max}) + m$ and $\log_{10}(N_\mu) = \log_{10}(N_\mu^{\max}) + n$, respectively.

$N_{c\mu}$ is linear with respect to the primary energy, as shown in Fig. 7. The reconstructed energy (E_{rec}) can be expressed as

$$E_{rec} = kN_{c\mu}, \quad (5)$$

where the parameter k is obtained by fitting the relationship between the primary energy and $N_{c\mu}$ of the light component, as shown in Fig. 7.

The resolution of the energy reconstructed using Eq. (5) is the sigma of the Gaussian fitting of the relative energy deviation $[(E_{rec} - E_{true})/E_{true}]$ distribution, whereas the bias of the reconstructed energy is the mean value of the distribution. As an example, the distribution of the relative energy deviation of the light component in the reconstructed energy (E_{rec}) range of $10^{6.1}$ – $10^{6.2}$ GeV is shown in Fig. 8. The bias and resolution of the energy reconstruction are also shown in this plot as the mean and sigma of the Gaussian fitting on this distribution, respectively.

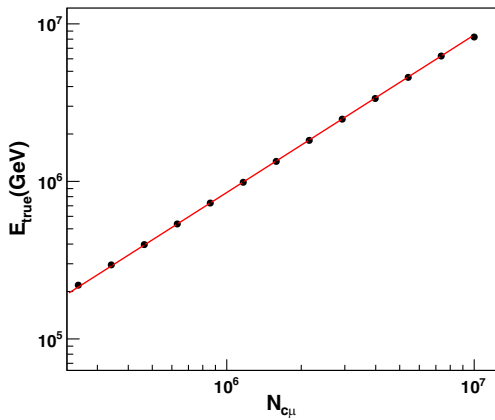


FIG. 7. E_{true} versus the $N_{c\mu}$ for light component of cosmic rays. The red line is the fitted result of the function $E_{true} = kN_{c\mu}$. The error bar is smaller than the dot size.

According to Eq. (5), the shower energy was reconstructed with this composite variable around the knee region from 300 TeV to 10 PeV for the light components. The resolution and bias of the energy reconstruction are shown in the left-hand plot of Fig. 9. The energy resolution was better than 10% at approximately 1 PeV, with an energy bias of less than 2%. This method of energy determination yielded systematic differences between the proton and helium of less than 1% above 300 TeV, as shown in Fig. 9 (right). The reconstructed energy resolutions of the proton and helium of the air showers improved with increase in the energy. Compared with the energy reconstruction using only Cherenkov light [4], this approach reduced the difference in the relative energy deviations between the proton and helium and improved the energy resolution as well.

To improve the energy reconstruction accuracy of the light mass component (proton and helium) further, $C = 140$ [in Eq. (4)] was optimized in this study, and the fit using Eq. (5) was repeated. The corresponding

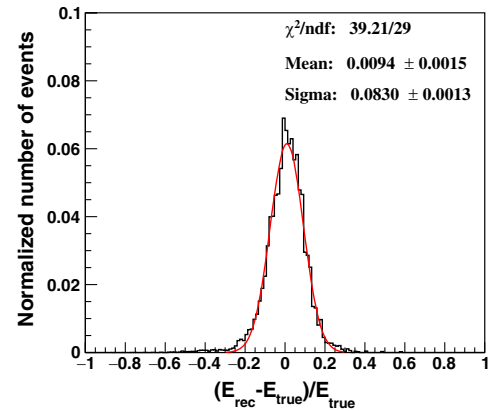


FIG. 8. Relative energy deviation distribution of light component in the reconstructed energy range $10^{6.1}$ – $10^{6.2}$ GeV. The red line is the fitted result of the Gaussian function. ndf is number of degree of freedom.

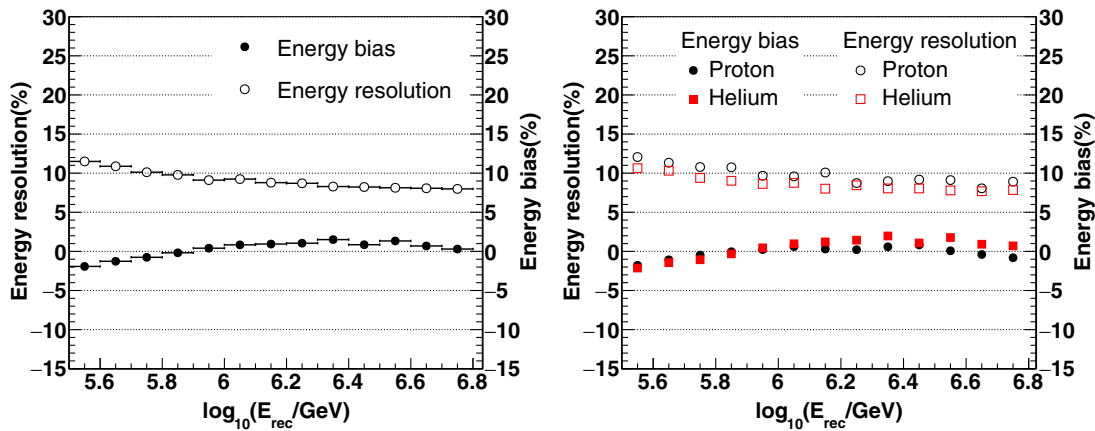


FIG. 9. Left: energy resolution (hollowed circles) and energy bias (solid circles) versus the E_{rec} of the light components. Right: the energy resolutions (hollowed shapes) and biases (solid shapes) of the proton (circles) and helium (squares) versus the E_{rec} . The results are based on an estimator with $C = 120$.

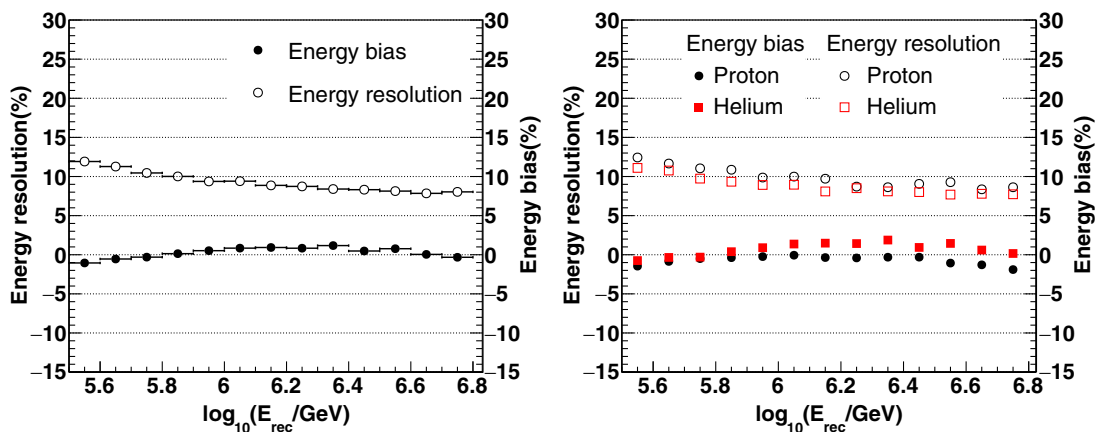


FIG. 10. Left: energy resolution (hollowed circles) and energy bias (solid circles) versus the E_{rec} of the light components. Right: the energy resolutions (hollowed shapes) and biases (solid shapes) of the proton (circles) and helium (squares) versus the E_{rec} . The results are based on an estimator with $C = 140$.

reconstructed energy of the light mass component is shown in Fig. 10. The energy resolution of the light mass component was less than 10% with an energy bias of less than 1% at approximately 1 PeV, and the difference in the energy bias between proton and helium was less than 1% at approximately 1 PeV.

C. Discussion

The heavier components were also investigated in this study. The $N_{c\mu}$ relationship with the primary energy for the heavy component (CNO, MgAlSi, and iron) is shown in the left panel of Fig. 11, together with proton and helium. As evident, this new estimator exhibited a linear relationship with the primary energy and was insensitive to the primary type of air showers.

With this method, the energy resolutions of all five mass components were better than 10% above 1 PeV, and the energy biases were within 3%, as shown in the right panel of Fig. 11. Further, as shown in Fig. 11, the energy

resolution improved with increasing energy of the air shower. The minimum difference in the energy bias between the proton and iron showers was less than 1% at 800 TeV, and the maximum difference in the energy bias was 7% at 6 PeV. The energy bias of iron is slightly larger than that of the proton, because parameters β [in Eq. (2)], C [in Eq. (4)], and k [in Eq. (5)] are somewhat mass dependent. Therefore, to improve the energy bias of iron as well as the proton, these parameters should be redetermined by fitting the iron shower.

The relationship between N_{pe} and R_p can be normalized using a linear function in Eq. (2) in the R_p range of 50–150 m. To extend the R_p far away, for example, 200 m, a more complicated Cherenkov lateral distribution function is required to describe the relationship [8].

The above results were based on the samples produced using the baseline hadronic interaction model QGSJET-II-04. A similar analysis was also performed with the alternative sample produced using the EPOS-LHC model [12].

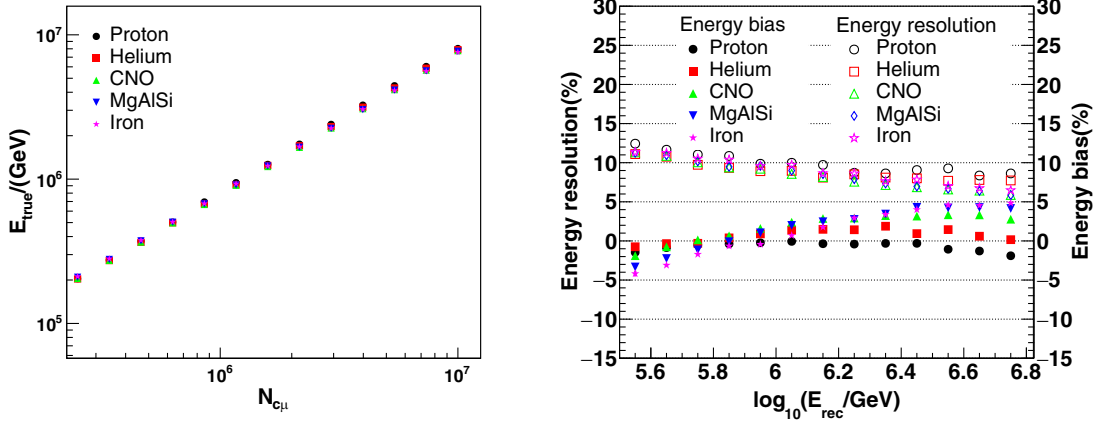


FIG. 11. Left: E_{true} versus the $N_{c\mu}$ for five mass components of air shower. Right: the reconstruction energy resolution and bias versus E_{rec} for the five groups of air shower. The hollowed and solid shapes stand for the resolution and the bias of reconstructed energy, respectively. Different shapes with different colors are described in the plot.

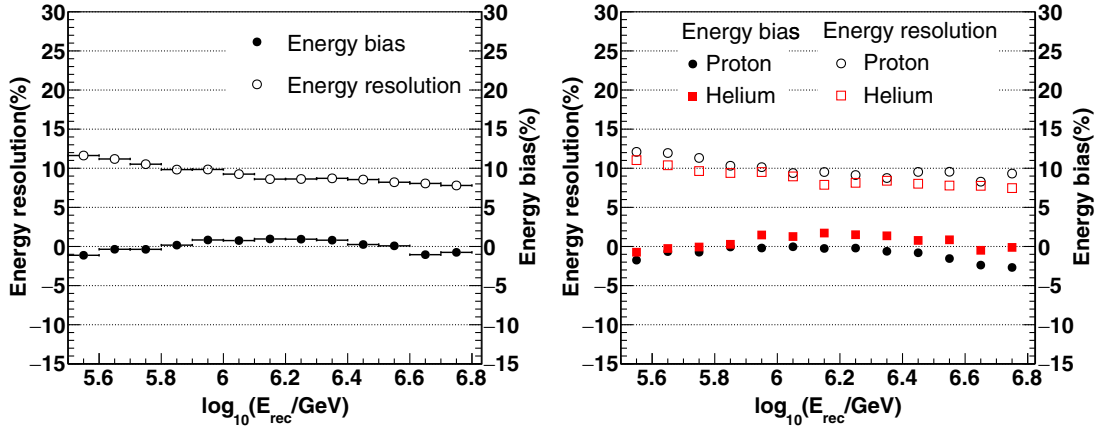


FIG. 12. Left: energy resolution (hollowed circles) and energy bias (solid circles) versus the E_{rec} of the light components. Right: the energy resolutions (hollowed shapes) and biases (solid shapes) of the proton (circles) and helium (squares) versus the E_{rec} . The MC simulation is based on the EPOS-LHC hadronic interaction model.

The energy reconstruction results based on the EPOS-LHC hadronic interaction model are presented in Fig. 12. The results of EPOS-LHC are similar to those of MC simulations based on QGSJET-II-04. The energy reconstruction function [Eq. (5)] was also used, but the parameter k was slightly different from the result obtained based on the QGSJET-II-04 hadronic interaction model. The difference in k is 3.5% between the two hadronic interaction models, which corresponds to the energy estimation uncertainty of 3.5%.

IV. SUMMARY

For the first time, we combine the Cherenkov lights and the number of muons to develop a new energy reconstruction method to measure the energy of air showers induced by the nucleus. The energy resolution for the light component was better than 10% with an energy bias of less than 1% at approximately 1 PeV. The difference in the

relative energy deviations was less than 1% for proton and helium at approximately 1 PeV. Compared with the case where only Cherenkov light is used in the energy reconstruction because the energy fraction remaining in the hadronic part of the air shower was added in the form of the number of muons in this work, the effects of the primary mass of the nuclear air showers on the reconstructed energy were effectively reduced and the reconstructed energy resolution was improved as well. Moreover, the energy resolutions of all components were better than 10%, within 3% of the energy biases of approximately 1 PeV. The energy reconstruction method proposed in this study can be used for high-precision single element, light component, heavy component, and all particle energy spectrum measurements.

ACKNOWLEDGMENTS

This work is supported in China by the National Key R&D program of China under Grants No. 2018YFA0404202 and

No. 2018YFA0404201. This research work is also supported by the National Natural Science Foundation of China, with NSFC Grants No. 12275280, No. 12105293, No. 12175121 and Sichuan Province Science Foundation for Distinguished

Young Scholars No. 2022JDJQ0043. We are grateful to the Chengdu Management Committee of Tianfu New Area for their constant financial support of research with LHAASO data.

-
- [1] T. Antoni *et al.* (KASCADE Collaboration), KASCADE measurements of energy spectra for elemental groups of cosmic rays: Results and open problems, *Astropart. Phys.* **24**, 1 (2005).
- [2] M. Amenomori *et al.* (Tibet AS γ Collaboration), Cosmic-ray energy spectrum around the knee obtained by the Tibet experiment and future prospects, *Adv. Space Res.* **47**, 629 (2011).
- [3] B. Bartoli *et al.* (ARGO-YBJ Collaboration), Cosmic ray proton plus helium energy spectrum measured by the ARGO-YBJ experiment in the energy range 3–300 TeV, *Phys. Rev. D* **91**, 112017 (2015).
- [4] B. Bartoli *et al.* (ARGO-YBJ and LHAASO Collaborations), Knee of the cosmic hydrogen and helium spectrum below 1 PeV measured by ARGO-YBJ and a Cherenkov telescope of LHAASO, *Phys. Rev. D* **92**, 092005 (2015).
- [5] H. He, Design of the LHAASO detectors, *Radiat. Detect. Technol. Methods* **2**, 1 (2018).
- [6] X.-H. Ma *et al.*, Chapter 1 LHAASO Instruments and Detector technology, *Chin. Phys. C* **46**, 030001 (2022).
- [7] F. Aharonian *et al.* (LHAASO Collaboration), Absolute calibration of LHAASO WFCTA camera based on LED, *Nucl. Instrum. Methods Phys. Res., Sect. A* **1021**, 165824 (2022).
- [8] F. Aharonian *et al.* (LHAASO Collaboration), Reconstruction of Cherenkov image by multiple telescopes of LHAASO-WFCTA, *Radiat. Detect. Technol. Methods* **6**, 544 (2022).
- [9] Z. Cao (LHAASO Collaboration), A future project at Tibet: The large high altitude air shower observatory (LHAASO), *Chin. Phys. C* **34**, 249 (2010).
- [10] D. Heck, J. Knapp, J. N. Capdevielle, G. Schatz, and T. Thouw, *CORSIKA: A Monte Carlo Code to Simulate Extensive Air Showers* (1998), 10.5445/IR/270043064.
- [11] S. Ostapchenko, QGSJET-II: Physics, recent improvements, and results for air showers, *EPJ Web Conf.* **52**, 02001 (2013).
- [12] T. Pierog, I. Karpenko, J. M. Katzy, E. Yatsenko, and K. Werner, EPOS LHC: Test of collective hadronization with data measured at the CERN Large Hadron Collider, *Phys. Rev. C* **92**, 034906 (2015).
- [13] T. K. Gaisser, T. Stanev, and S. Tilav, Cosmic ray energy spectrum from measurements of air showers, *Front. Phys.* **8**, 748 (2013).
- [14] S. Chen, Detector Simulation of LHAASO-KM2A with GEANT4, *Proc. Sci., ICRC2019* (2021) 219.
- [15] S. Agostinelli *et al.* (GEANT4 Collaboration), GEANT4—a simulation toolkit, *Nucl. Instrum. Methods Phys. Res., Sect. A* **506**, 250 (2003).
- [16] F. Aharonian *et al.*, The observation of the Crab Nebula with LHAASO-KM2A for the performance study, *Chin. Phys. C* **45**, 025002 (2021).
- [17] H. Zhang, H. He, and C. Feng, Approaches to composition independent energy reconstruction of cosmic rays based on the LHAASO-KM2A detector, *Phys. Rev. D* **106**, 123028 (2022).
- [18] T. Ergin, *The Energy Spectrum of Very High Energy Gamma Rays from the Crab Nebula as Measured by the H.E.S.S. Array* (2005), 10.18452/15435.
- [19] J. R. Horandel, Cosmic rays from the knee to the second knee: 10^4 to 10^{18} eV, *Mod. Phys. Lett. A* **22**, 1533 (2007).
- [20] A. Haungs, H. Rebel, and M. Roth, Energy spectrum and mass composition of high-energy cosmic rays, *Rep. Prog. Phys.* **66**, 1145 (2003).
- [21] J. Matthews, A Heitler model of extensive air showers, *Astropart. Phys.* **22**, 387 (2005).
- [22] J. Alvarez-Muniz, R. Engel, T. K. Gaisser, J. A. Ortiz, and T. Stanev, Hybrid simulations of extensive air showers, *Phys. Rev. D* **66**, 033011 (2002).
- [23] K.-H. Kampert and M. Unger, Measurements of the cosmic ray composition with air shower experiments, *Astropart. Phys.* **35**, 660 (2012).
- [24] E. E. Korosteleva, V. V. Prosin, L. A. Kuzmichev, and G. Navarra, Measurement of cosmic ray primary energy with the atmospheric Cherenkov light technique in extensive air showers, *Nucl. Phys. B, Proc. Suppl.* **165**, 74 (2007).
- [25] W. D. Apel *et al.* (KASCADE-Grande Collaboration), Probing the evolution of the EAS muon content in the atmosphere with KASCADE-Grande, *Astropart. Phys.* **95**, 25 (2017).